Experimental Study of Cold-Formed Ferritic Stainless Steel Hollow Sections

S. Afshan[1] and L. Gardner[2]

Abstract: Stainless steel is gaining increasing use in construction because of its durability, favorable mechanical properties, and aesthetic appearance, with the austenitic grades being the most commonly used. Austenitic stainless steels have a high nickel content (8–11%), resulting in high initial material cost and significant price fluctuations; this, despite its desirable properties, represents a considerable disadvantage in terms of material selection. Ferritic stainless steels, having no or very low nickel content, may offer a more viable alternative for structural applications, reducing both the level and variability of the initial material cost while maintaining adequate corrosion resistance. There is currently limited information available on the structural performance of this type of stainless steel. Therefore, to overcome this limitation, a series of material, cross section, and member tests have been performed, covering both the standard EN 1.4003 grade (similar to the chromium weldable structural steel 3Cr12) and the EN 1.4509 grade (441), which has improved weldability and corrosion resistance. In total, 20 tensile coupon tests, 16 compressive coupon tests, eight stub column tests, 15 flexural buckling tests, and eight in-plane bending tests were carried out. Precise measurements of the geometric properties of the test specimens, including the local and global geometric imperfections, were also made. The experimental results are used to assess the applicability of the current European (EN 1993-1-4) and North American (SEI/ASCE-8) provisions to ferritic stainless steel structural components. In addition, the relative structural performance of ferritic stainless steel to that of more commonly used stainless steel grades is also presented, showing ferritic stainless steel to be an attractive choice for structural applications.
DOI: 10.1061/(ASCE)ST.1943-541X.0000580.

CE Database subject headings: Beams; Buckling; Cold-formed steel; Columns; Cross sections; Hollow sections; Laboratory tests; Stainless steel; Experimentation.

Author keywords: Cold-formed steel; Laboratory tests; Stainless steel.

Introduction

The physical and mechanical characteristics of stainless steel such as high strength, stiffness and ductility, weldability, durability, good fire resistance, and ready reuse and recycling make it suitable for a range of architectural and structural applications. The austenitic EN 1.4301 and EN 1.4401 (304 and 316) grades, containing 17–18% chromium and 8–11% nickel, are most commonly used in construction. Both grades have a minimum specified design strength (0.2% proof strength) of 210–240 N/mm^2 [EN 10088-4; European Committee for Standardization (CEN) 2009b]. The high nickel content of the austenitic grades provides a number of positive attributes, such as very good ductility and elevated temperature performance, but the resulting high initial material cost is a significant disincentive for material selection.

Ferritic stainless steels, having no or very low nickel content, may offer a more viable alternative for structural applications, because of their lower initial material cost and improved price stability. The main alloying element is chromium, with contents typically between 11 and 18% (EN 10088-4; CEN 2009b). These steels are easier to work and machine than the austenitic grades and have a higher yield strength in the annealed condition of 250–330 N/mm^2. Furthermore, by varying the chromium content (10.5–29%), and with additions of other alloying elements, the required corrosion resistance for a wide range of structural applications and operating environments can be achieved. Stabilized ferritic grades, with additions of titanium and niobium alloying elements, such as EN 1.4509 (441) and EN 1.4521 (444), are broadly similar in terms of corrosion resistance to the EN 1.4301 and EN 1.4401 austenitic grades.

Ferritic stainless steel has been widely used in various applications in the automotive industry, road and rail transport, power generation, and mining, although its structural use has remained relatively scarce. Despite some previous research (van den Berg 2000) and inclusion of the three traditional ferritic grades, EN 1.4003 (similar to chromium weldable structural steel 3Cr12), EN 1.4016 (430), and EN 1.4512 (409), in Eurocode 3: Part 1-4 (CEN 2006a), their structural performance requires further verification, particularly for the case of hollow sections. Hence, the focus of the present paper is to describe a comprehensive laboratory testing program on Grades EN 1.4003 and EN 1.4509 stainless steel square and rectangular hollow sections (SHS and RHS, respectively), which has been recently conducted at Imperial College London. To determine the material properties, a total of 20 tensile coupon tests, including both flat and corner specimens, and 16 compressive coupon tests were performed. At the cross section level, eight stub column tests and eight in-plane bending tests, including three-point bending and four-point bending configurations, have been carried out. At member level, 15 column flexural buckling tests have been conducted. The experimental results obtained are reported, analyzed, and compared with the results of tests performed on other stainless steel grades. Finally, design recommendations suitable for incorporation into European (EN 1993-1-4; CEN 2006a)

[1]Ph.D. Student, Dept. of Civil and Environmental Engineering, Imperial College London, London SW7 2AZ, U.K. (corresponding author). E-mail: sheida.afshan06@imperial.ac.uk

[2]Reader, Dept. of Civil and Environmental Engineering, Imperial College London, London SW7 2AZ, U.K. E-mail: leroy.gardner@imperial.ac.uk

Note. This manuscript was submitted on September 1, 2011; approved on February 8, 2012; published online on April 15, 2013. Discussion period open until October 1, 2013; separate discussions must be submitted for individual papers. This paper is part of the ***Journal of Structural Engineering***, Vol. 139, No. 5, May 1, 2013. ©ASCE, ISSN 0733-9445/2013/5-717–728/$25.00.

and North American (SEI/ASCE-8; ASCE 2002) standards have been proposed.

Experimental Studies

Introduction

A laboratory testing program comprising 36 material tests, eight stub column tests, eight bending tests, and 15 flexural buckling tests was conducted at Imperial College London to investigate the structural performance of cold-formed ferritic stainless steel tubular structural elements. Four section sizes were examined: RHS $120 \times 80 \times 3$, RHS $60 \times 40 \times 3$, SHS $80 \times 80 \times 3$, and SHS $60 \times 60 \times 3$. The first three sections were of the standard EN 1.4003 grade, whereas SHS $60 \times 60 \times 3$ was Grade EN 1.4509, which has improved weldability and corrosion resistance. The chemical compositions and the tensile properties of the coil material from which the specimens were formed, as provided by the mill certificates, are presented in Tables 1 and 2, respectively. No chemical composition details were available for Grade EN 1.4509 SHS $60 \times 60 \times 3$ specimens. The notation used in Table 2 is as follows: $\sigma_{0.2}$ is the 0.2% proof stress, $\sigma_{1.0}$ is the 1% proof stress, σ_u is the ultimate tensile stress, and ε_f is the tensile strain at fracture.

Material Tests

A series of tensile and compressive coupon tests was conducted to determine the basic engineering stress-strain response of the SHS and RHS ferritic specimens. All material was extracted from the same lengths of tube as the stub column, long column, and beam specimens. One tensile flat and one compressive flat coupon were machined from each of the four faces of the SHS and RHS specimens in the longitudinal direction, resulting in a total of 16 tensile coupon tests and 16 compressive coupon tests. All tensile coupons were parallel necked specimens with a neck length of 150 mm and width of 20 mm, whereas the compressive coupons were of nominal dimensions 72×16 mm. Stainless steel exhibits pronounced strain hardening, resulting in the corner regions of cold-formed sections having a higher strength than that of the flat material (Ashraf et al. 2005). To investigate the extra degree of strength in the cold-worked corner regions, tensile tests on corner coupons, with nominal length of 320 mm, extracted from the curved portions of each of the cold-formed sections, were also conducted.

The tests were performed using an Instron 8802 250 kN hydraulic testing machine, in accordance with EN ISO 6892-1 (CEN 2009a).

Table 1. Chemical Composition of Grade EN 1.4003 Stainless Steel Specimens

Section	C (%)	Si (%)	Mn (%)	P (%)	S (%)	Cr (%)	Ni (%)	N (%)
RHS $120 \times 80 \times 3$	0.005	0.50	1.44	0.029	0.002	11.3	0.4	0.01
RHS $60 \times 40 \times 3$	0.010	0.37	1.46	0.029	0.003	11.2	0.5	0.01
SHS $80 \times 80 \times 3$	0.010	0.25	1.43	0.028	0.003	11.3	0.4	0.01

Table 2. Mechanical Properties as Stated in the Mill Certificates

Section	Grade	$\sigma_{0.2,\text{mill}}$ (N/mm^2)	$\sigma_{1.0,\text{mill}}$ (N/mm^2)	$\sigma_{u,\text{mill}}$ (N/mm^2)	ε_f (%)
RHS $120 \times 80 \times 3$	EN 1.4003	346	368	498	42
RHS $60 \times 40 \times 3$	EN 1.4003	339	360	478	38
SHS $80 \times 80 \times 3$	EN 1.4003	321	343	462	45

Strain control was used to drive the testing machine at a strain rate of 0.002%/s up to the 0.2% proof stress and 0.005%/s until fracture for the tensile coupon tests. A uniform displacement rate of 0.07 mm/min was used for the compressive coupon tests. For the tensile coupon tests, an optical extensometer was used to measure the longitudinal strain over a gauge length of 100 mm while two linear electrical resistance strain gauges attached to the edges of the compressive coupons were used to measure the strain. Static loads were obtained at key stages by holding the cross head of the testing machine for a duration of 2 min to allow stress relaxation to take place. Buckling of the compressive coupons was prevented by means of a bracing jig. Load, strain, and other relevant variables were all recorded at 1-s intervals using the fully integrated modular software package *Blue-hill 2*.

The obtained material data for each specimen are given in Table 3, whereas the weighted average (based on face width) tensile and compressive material properties of each section are given in Tables 4 and 5, respectively. The coupon designation begins with the section size, e.g., SHS $80 \times 80 \times 3$, followed by the test type, TF for tensile flat, CF for compressive flat, and TC for tensile corner, and finally the section face number (1, 2, 3, or 4), as explained in Fig. 1. The material parameters reported in Tables 3 and 4 are the Young's modulus E, the static 0.2% proof stress $\sigma_{0.2}$, the static 1% proof stress $\sigma_{1.0}$, the static ultimate tensile stress σ_u, the plastic strain at fracture ε_f (based on elongation over the standard gauge length equal to $5.65\sqrt{A_c}$, where A_c is the cross-sectional area of the coupon), and the strain-hardening exponents n and $n'_{0.2,1.0}$ used in the compound Ramberg-Osgood material model (Mirambell and Real 2000; Rasmussen 2003; Ashraf et al. 2006). The early region of the stress-strain curve that was affected by the initial curvature of the coupons was not considered for the calculation of the Young's modulus. The measured tensile stress-strain curves, up to 1% tensile strain, are depicted in Figs 2–5.

Stub Column Tests

Stub column tests on four ferritic stainless steel sections, RHS $120 \times 80 \times 3$, RHS $60 \times 40 \times 3$, SHS $80 \times 80 \times 3$, and SHS $60 \times 60 \times 3$, were performed. Two repeated concentric compression tests were carried out for each section size. Stub column lengths were selected to be short enough to avoid overall flexural buckling but still long enough to provide a representative pattern of geometric imperfections and residual stresses (Galambos 1998). The chosen nominal lengths were equal to three times the larger nominal cross-sectional dimension for the RHS $120 \times 80 \times 3$, SHS $80 \times 80 \times 3$, and SHS $60 \times 60 \times 3$ specimens. A shorter length, equal to two times the larger nominal cross-sectional dimension, was used for RHS $60 \times 40 \times 3$ specimens, because evidence of global buckling was observed in the failure modes of longer specimens.

The ends of the stub column specimens were milled flat and square to ensure uniform loading distribution during testing. The specimens were compressed between parallel platens in an Instron 3,500-kN hydraulic testing machine. The test setup was displacement controlled. The instrumentation consisted of one LVDT to measure the end shortening between the flat platens, a load cell to accurately record the applied load, and four linear electrical resistance strain gauges. The strain gauges were affixed to each specimen at midheight and at a distance four times the material thickness from the corners. All data, including load, displacement, strain, and voltage, were recorded at 1-s intervals using the data acquisition equipment DATASCAN and logged using the DSLOG computer package.

The average measured geometric dimensions of each stub column specimen are provided in Table 6, where L is the stub column length, h is the section depth, b is the section width, t is the thickness, and r_i is the average internal corner radius (Fig. 1). Initial local geometric imperfection magnitudes were not measured specifically for each test specimen but were measured over a representative 800-mm length of

J. Struct. Eng. 2013.139:717-728.

Table 3. Coupon Test Results for Each Specimen

Specimen reference	E (N/mm^2)	$\sigma_{0.2}$ (N/mm^2)	$\sigma_{1.0}$ (N/mm^2)	σ_u (N/mm^2)	ε_f (%)	R-O coefficients	
						n	$n'_{0.2,1.0}$
RHS 120 × 80 × 3-TF1	210,000	450	472	477	33	8.8	6.3
RHS 120 × 80 × 3-TF2	215,000	385	405	443	40	8.0	2.3
RHS 120 × 80 × 3-TF3	218,000	390	413	458	40	11.2	2.6
RHS 120 × 80 × 3-TF4	220,000	510	—[a]	535	23	12.6	8.2
RHS 120 × 80 × 3-TC	226,000	535	—[a]	554	13	6.0	—
RHS 120 × 80 × 3-CF1	213,000	439	478	—	—	5.6	2.4
RHS 120 × 80 × 3-CF2	215,000	372	415	—	—	6.9	4.1
RHS 120 × 80 × 3-CF3	210,000	362	415	—	—	5.2	3.2
RHS 120 × 80 × 3-CF4	205,000	487	537	—	—	5.3	2.5
RHS 60 × 40 × 3-TF1	220,000	438	—[a]	460	18	8.0	8.2
RHS 60 × 40 × 3-TF2	225,000	455	—[a]	481	28	9.4	9.8
RHS 60 × 40 × 3-TF3	210,000	435	—[a]	440	32	7.3	9.9
RHS 60 × 40 × 3-TF4	225,000	500	—[a]	542	21	6.4	8.9
RHS 60 × 40 × 3-TC	200,000	545	—[a]	597	10	4.7	—
RHS 60 × 40 × 3-CF1	215,000	423	465	—	—	5.5	2.2
RHS 60 × 40 × 3-CF2	220,000	425	495	—	—	7.2	2.7
RHS 60 × 40 × 3-CF3	220,000	400	454	—	—	7.6	4.3
RHS 60 × 40 × 3-CF4	210,000	429	486	—	—	5.0	3.8
SHS 80 × 80 × 3-TF1	220,000	435	—[a]	440	36	9.1	9.6
SHS 80 × 80 × 3-TF2	200,000	425	435	447	36	10.1	6.2
SHS 80 × 80 × 3-TF3	210,000	400	418	432	38	7.7	3.1
SHS 80 × 80 × 3-TF4	210,000	465	—[a]	470	31	7.7	10.0
SHS 80 × 80 × 3-TC	220,000	512	—[a]	520	11	7.8	—
SHS 80 × 80 × 3-CF1	215,000	413	475	—	—	7.4	2.4
SHS 80 × 80 × 3-CF2	210,000	398	443	—	—	5.1	2.5
SHS 80 × 80 × 3-CF3	215,000	375	423	—	—	7.4	2.7
SHS 80 × 80 × 3-CF4	205,000	429	483	—	—	5.4	2.7
SHS 60 × 60 × 3-TF1	220,000	540	—[a]	560	14	7.2	10.4
SHS 60 × 60 × 3-TF2	220,000	515	—[a]	524	20	8.6	9.9
SHS 60 × 60 × 3-TF3	223,000	502	—[a]	513	19	8.0	10.3
SHS 60 × 60 × 3-TF4	210,000	520	—[a]	538	13	7.4	12.5
SHS 60 × 60 × 3-TC	225,000	580	—[a]	665	13	4.3	9.5
SHS 60 × 60 × 3-CF1	215,000	492	542	—	—	6.4	4.6
SHS 60 × 60 × 3-CF2	215,500	465	509	—	—	6.5	2.3
SHS 60 × 60 × 3-CF3	210,000	478	524	—	—	6.9	2.8
SHS 60 × 60 × 3-CF4	220,000	497	550	—	—	5.5	2.5

[a]Ultimate tensile stress preceded the 1% proof stress.

Table 4. Weighted Average Tensile Flat Material Properties

Specimen reference	E (N/mm^2)	$\sigma_{0.2}$ (N/mm^2)	σ_u (N/mm^2)	ε_f (%)	R-O coefficients	
					n	$n'_{0.2,1.0}$
RHS 120 × 80 × 3	216,000	423	472	34	10.2	4.9
RHS 60 × 40 × 3	219,300	454	475	24	7.8	9.2
SHS 80 × 80 × 3	210,000	431	447	35	8.7	7.2
SHS 60 × 60 × 3	218,300	519	534	16	7.8	10.8

Table 5. Weighted Average Compressive Flat Material Properties

Specimen reference	E (N/mm^2)	$\sigma_{0.2}$ (N/mm^2)	$\sigma_{1.0}$ (N/mm^2)	R-O coefficients	
				n	$n'_{0.2,1.0}$
RHS 120 × 80 × 3	211,150	404	451	5.8	3.1
RHS 60 × 40 × 3	217,200	417	475	6.4	3.3
SHS 80 × 80 × 3	211,250	404	456	6.3	2.6
SHS 60 × 60 × 3	215,130	483	531	6.3	3.1

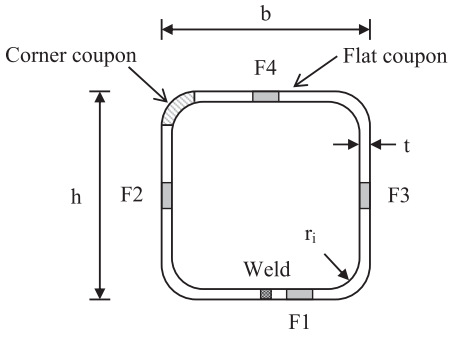

Fig. 1. Location of flat and corner coupons and definition of cross section symbols

each section size, following the procedures of Schafer and Peköz (1998). The maximum deviations from a flat datum were recorded for the four faces of each section and then averaged to give the imperfection magnitudes w_0 reported in Table 6.

J. Struct. Eng. 2013.139:717-728.

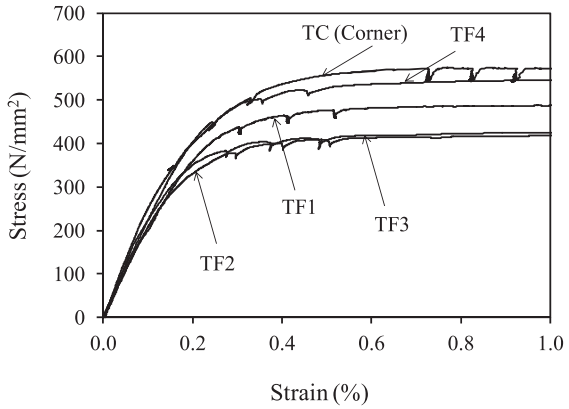

Fig. 2. RHS 120 × 80 × 3 tensile stress-strain curves

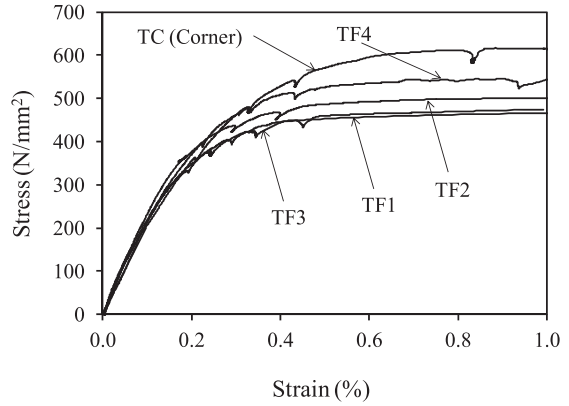

Fig. 3. RHS 60 × 40 × 3 tensile stress-strain curves

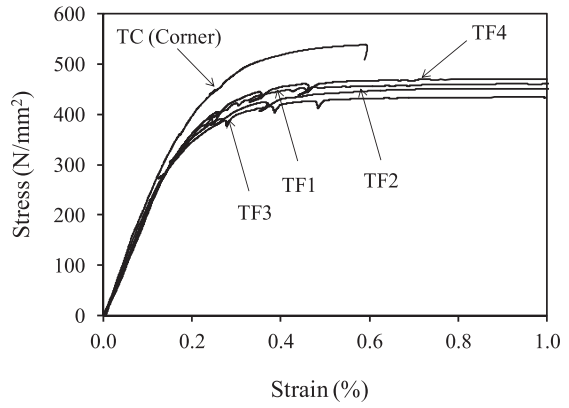

Fig. 4. SHS 80 × 80 × 3 tensile stress-strain curves

The static ultimate load N_u and the corresponding end shortening at ultimate load δ_u are given in Table 7. All test specimens failed by local buckling of the flat elements comprising the section. Fig. 6 shows typical failure modes. Tests were continued beyond the ultimate load, and the postultimate response was recorded. Full load-end shortening curves for the tested specimens are depicted in Fig. 7. Relevant guidelines provided by the Centre for Advanced Structural Engineering (1990) were used to eliminate elastic deformation of the end platens from the end shortening measurements. Hence, the true deformations of the stub columns were determined and used throughout the study.

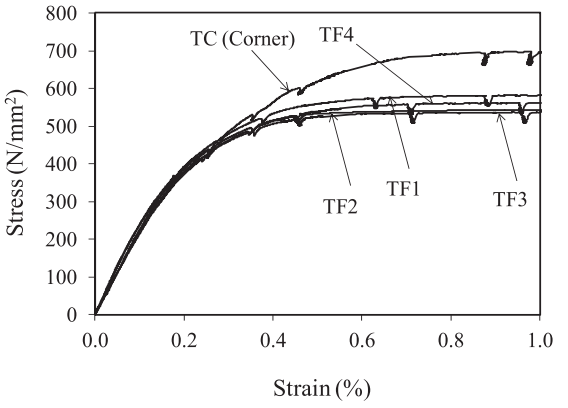

Fig. 5. SHS 60 × 60 × 3 tensile stress-strain curves

Table 6. Measured Dimensions of the Stub Column Specimens

Specimen	L (mm)	H (mm)	B (mm)	t (mm)	r_i (mm)	w_0 (mm)	A (mm^2)
RHS 120 × 80 × 3-SC1	362.0	119.9	80.0	2.84	3.70	0.061	1077.9
RHS 120 × 80 × 3-SC2	362.2	120.0	80.0	2.83	3.90	0.061	1074.3
RHS 60 × 40 × 3-SC1	122.1	59.9	40.0	2.81	3.19	0.081	508.1
RHS 60 × 40 × 3-SC2	122.1	59.9	40.0	2.81	3.19	0.081	508.0
SHS 80 × 80 × 3-SC1	242.0	80.1	80.1	2.83	3.67	0.087	850.8
SHS 80 × 80 × 3-SC2	242.0	80.1	80.1	2.82	3.43	0.087	849.1
SHS 60 × 60 × 3-SC1	182.2	60.5	60.5	2.98	2.90	0.061	662.1
SHS 60 × 60 × 3-SC2	182.2	60.5	60.6	2.90	3.10	0.061	654.8

Table 7. Summary of Test Results for Stub Columns

Specimen	Ultimate load N_u (kN)	End shortening at ultimate load δ_u (mm)
RHS 120 × 80 × 3-SC1	449	1.16
RHS 120 × 80 × 3-SC2	441	1.19
RHS 60 × 40 × 3-SC1	278	2.18
RHS 60 × 40 × 3-SC2	271	2.12
SHS 80 × 80 × 3-SC1	392	1.42
SHS 80 × 80 × 3-SC2	389	1.49
SHS 60 × 60 × 3-SC1	376	1.92
SHS 60 × 60 × 3-SC2	370	1.94

Beam Tests

A total of eight in-plane bending tests, in two configurations, were conducted to investigate the cross section response of SHS and RHS ferritic stainless steel beams under constant moment (four-point bending) and a moment gradient (three-point bending). All specimens had a total length of 1,700 mm and were simply supported between two steel rollers, which were placed 100 mm inward from the ends of the beams and allowed axial displacement of the beam's ends, resulting in a span of 1,500 mm.

The tested beams were loaded symmetrically, in an Instron 2,000-kN hydraulic testing machine, at the third points and at midspan for the four-point bending and the three-point bending arrangements, respectively, as shown in Figs. 8 and 9. String potentiometers were located at the loading points to measure the vertical deflections, and for the three-point bending tests, two inclinometers were also positioned at each end of the beam specimens to measure end rotations. Linear electrical resistance strain gauges were affixed to the extreme tensile and compressive fibers of the section at midspan and at 100 mm distance from

J. Struct. Eng. 2013.139:717-728.

the midspan for the four-point bending and for the three-point bending tests, respectively. Wooden blocks were placed within the tubes at the loading points to prevent web crippling. The test setup was displacement controlled at a rate of 2 mm/min. Load, displacement, strain, end rotation, and input voltage were all recorded using the data acquisition equipment DATASCAN and logged using the DSLOG computer package.

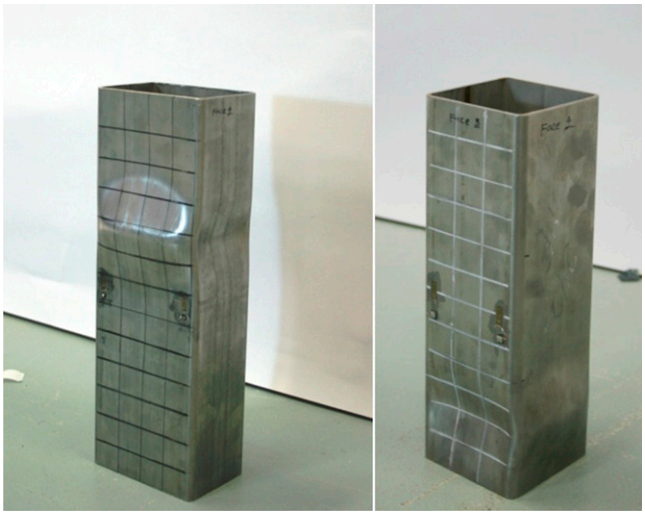

Fig. 6. Typical stub column failure mode

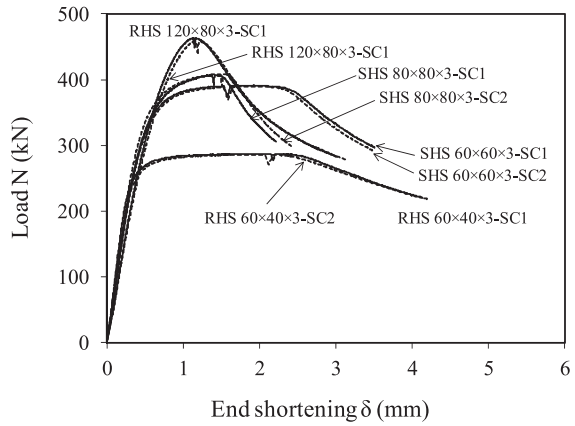

Fig. 7. Load end-shortening curves for stub columns

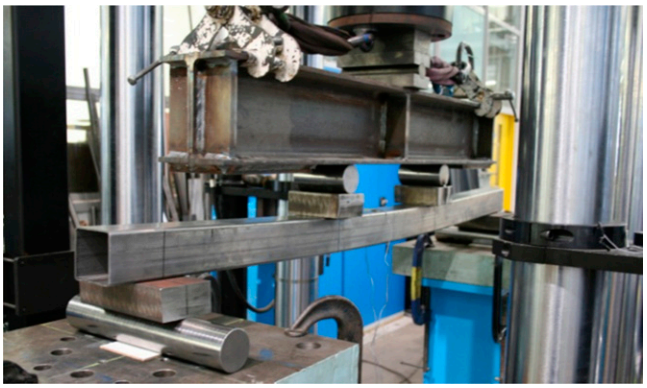

Fig. 8. Bending test setup (4PB)

Average measured dimensions of the beam specimens, together with the maximum local imperfections w_0, are reported in Table 8. The static ultimate test bending moment M_u and the cross section rotation capacity R are reported in Table 9. The obtained moment-curvature and midspan moment-rotation curves from the four-point and three-point bending tests are shown in Figs. 10 and 11, respectively, where M_u is the ultimate test moment, M_{pl} is the plastic moment capacity, θ is the midspan rotation, taken as the sum of the two end rotations from the inclinometer measurements, θ_{pl} is the elastic component of the rotation at M_{pl}, κ is the curvature, and κ_{pl} is the elastic curvature corresponding to M_{pl}. The curvature was evaluated using Eq. (1), where D_{midspan} is the vertical deflection at midspan, D_{average} is the average vertical displacement at the loading points, and L_{midspan} is the length between the loading points. Rotation capacity was calculated as $R = (\kappa_u/\kappa_{pl}) - 1$ and $R = (\theta_u/\theta_{pl}) - 1$ for the four-point bending and three-point bending tests, respectively, where κ_u (θ_u) is the curvature (rotation) at which the moment-curvature (moment-rotation) curve falls below M_{pl} on the descending branch, and κ_{pl} (θ_{pl}) is

Fig. 9. Bending test setup (3PB)

Table 8. Measured Dimensions of the Beam Specimens

Specimen	Axis of bending	L (mm)	H (mm)	B (mm)	T (mm)	r_i (mm)	w_0 (mm)
RHS 120 × 80 × 3-4PB	Major	1,500	120.0	79.9	2.84	3.78	0.061
RHS 60 × 40 × 3-4PB	Major	1,500	60.2	39.9	2.86	3.15	0.081
SHS 80 × 80 × 3-4PB	—	1,500	80.4	80.0	2.80	3.95	0.087
SHS 60 × 60 × 3-4PB	—	1,500	60.7	60.7	2.89	2.86	0.061
RHS 120 × 80 × 3-3PB	Major	1,500	119.9	79.9	2.83	3.80	0.061
RHS 60 × 40 × 3-3PB	Major	1,500	60.4	40.8	2.82	3.18	0.081
SHS 80 × 80 × 3-3PB	—	1,500	80.5	80.2	2.81	3.81	0.087
SHS 60 × 60 × 3-3PB	—	1,500	60.6	60.5	2.87	2.88	0.061

Table 9. Summary of Test Results for Beams

Specimen	Axis of bending	Ultimate moment M_u (kNm)	Rotation capacity R
RHS 120 × 80 × 3-4PB	Major	20.0	1.45
RHS 60 × 40 × 3-4PB	Major	5.3	>4.90
SHS 80 × 80 × 3-4PB	—	11.3	1.86
SHS 60 × 60 × 3-4PB	—	7.9	2.85
RHS 120 × 80 × 3-3PB	Major	21.1	1.30
RHS 60 × 40 × 3-3PB	Major	5.9	>4.10
SHS 80 × 80 × 3-3PB	—	11.4	1.12
SHS 60 × 60 × 3-3PB	—	8.4	2.15

J. Struct. Eng. 2013.139:717-728.

the elastic curvature (rotation) corresponding to M_{pl} on the ascending branch. All test specimens failed by local buckling of the compression flange

$$\kappa = \frac{8\left(D_{\text{midspan}} - D_{\text{average}}\right)}{4\left(D_{\text{midspan}} - D_{\text{average}}\right)^2 + L_{\text{midspan}}{}^2} \tag{1}$$

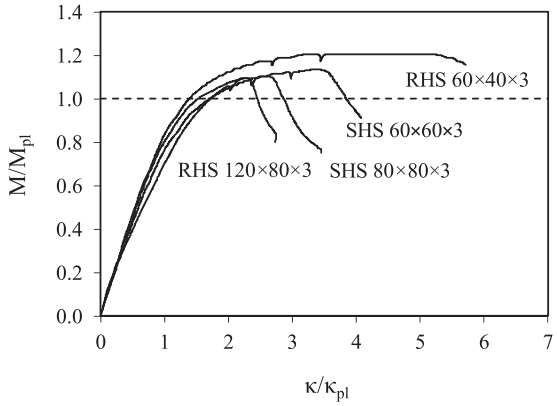

Fig. 10. Normalized moment-curvature results (four-point bending)

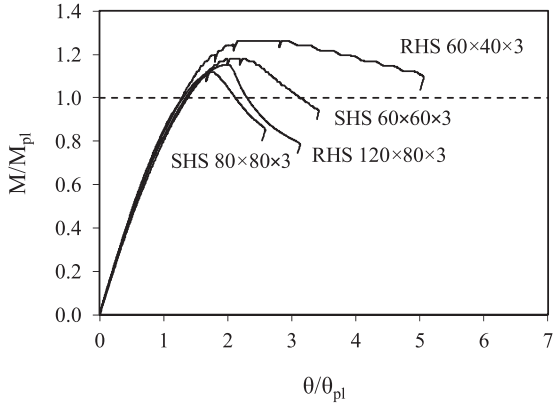

Fig. 11. Normalized moment-rotation results (three-point bending)

Flexural Buckling Tests

Column tests on ferritic stainless steel members, with the same nominal cross-sectional dimensions as examined for stub columns and beams, RHS $120 \times 80 \times 3$, RHS $60 \times 40 \times 3$, SHS $80 \times 80 \times 3$, and SHS $60 \times 60 \times 3$, were carried out to investigate the flexural buckling response of SHS and RHS pin-ended compression members under axial loading. Different column lengths of nominal dimensions 1.1, 1.6, 2.1, and 2.6 m were tested, providing a spectrum of nondimensional member slenderness $\overline{\lambda}$, defined in accordance with EN 1993-1-4 (CEN 2006a) [see Eq. (2)], ranging from 0.31 to 2.33

$$\overline{\lambda} = \sqrt{\frac{A\sigma_{0.2}}{N_{cr}}} \tag{2}$$

where A = cross-sectional area, taken as the gross cross-sectional area for fully effective sections and the effective cross-sectional area A_{eff} for slender sections; $\sigma_{0.2}$ = 0.2% proof stress; and N_{cr} = elastic buckling load of the column.

Measurements of the geometries of the column specimens and the initial global geometric imperfections were conducted before testing and are provided in Table 10, where symbols are as previously defined in Fig. 1, and ω_0 is the measured global imperfection amplitude in the axis of buckling. The general test setup configuration is depicted in Fig. 12. The specimens were loaded in an Instron 2,000-kN hydraulic testing machine through hardened steel knife edges at both ends to provide pinned end conditions about the axis of buckling and fixed conditions about the orthogonal axis, as shown in Fig. 12. Displacement control was used to drive the hydraulic machine at a constant rate of 0.5 mm/min. For column specimens where the measured global imperfection was less than $L/1{,}500$, where L is the pin-ended column buckling length (taken as the total distance between the steel knife edges), an eccentricity of loading was applied such that the combined effects of the measured imperfection and the loading eccentricity was equal to $L/1{,}500$. For other tests, the load was applied concentrically because the measured global imperfections were greater than $L/1{,}500$.

The instrumentation consisted of a string potentiometer to measure the midheight lateral deflection in the axis of buckling, inclinometers positioned at each end of the members to measure the end rotations about the axis of buckling, and four linear electrical resistance strain gauges affixed to the extreme tensile and compressive fibers of the section at midheight and at a distance of four times the material

Table 10. Measured Dimensions of the Flexural Buckling Specimens

Specimen	L (mm)	h (mm)	b (mm)	t (mm)	r_i (mm)	ω_0 (mm)	A (mm^2)
RHS $120 \times 80 \times 3$-1077	1,077	120.0	79.9	2.87	3.88	0.95	1,088.0
RHS $120 \times 80 \times 3$-1577	1,577	120.0	79.9	2.81	3.57	0.96	1,065.5
RHS $120 \times 80 \times 3$-2077	2,077	120.0	79.8	2.78	4.10	1.05	1,053.4
RHS $120 \times 80 \times 3$-2577	2,577	119.7	79.8	2.73	3.90	1.10	1,034.3
RHS $60 \times 40 \times 3$-1177	1,177	59.9	39.9	2.79	3.21	1.12	504.3
RHS $60 \times 40 \times 3$-1577	1,577	59.9	39.8	2.72	3.40	1.09	491.3
RHS $60 \times 40 \times 3$-2077	2,077	59.9	39.9	2.79	3.21	1.05	503.5
RHS $60 \times 40 \times 3$-2577	2,577	59.9	39.9	2.76	3.36	0.95	498.8
SHS $80 \times 80 \times 3$-1577	1,577	80.1	80.0	2.79	3.59	1.15	838.2
SHS $80 \times 80 \times 3$-2077	2,077	80.0	79.8	2.79	3.97	1.05	833.4
SHS $80 \times 80 \times 3$-2577	2,577	80.1	79.8	2.78	3.48	1.05	833.2
SHS $60 \times 60 \times 3$-1177	1,177	60.4	60.4	2.85	2.90	1.25	634.9
SHS $60 \times 60 \times 3$-1577	1,577	60.6	60.5	2.82	2.93	1.15	629.6
SHS $60 \times 60 \times 3$-2077	2,077	60.5	60.4	2.86	3.02	1.10	637.3
SHS $60 \times 60 \times 3$-2577	2,577	60.6	60.6	2.91	3.09	1.15	647.8

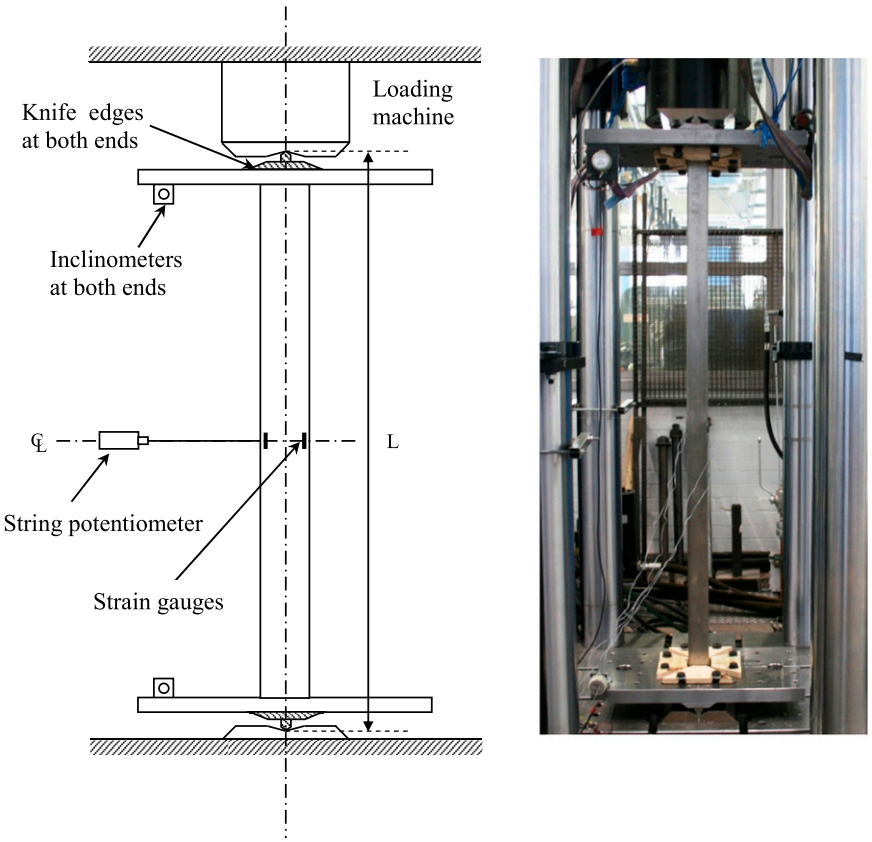

(a) Schematic diagram of the test set-up (b) Experimental set-up

(c) Steel Knife-edge arrangement

Fig. 12. Flexural buckling test setup

thickness from the corners. Applied load and vertical displacement were obtained directly from the loading machine. Load, strain, lateral and vertical displacements, end rotations, and input voltage were all recorded using the data acquisition equipment DATASCAN and logged using the DSLOG computer package. All data were recorded at 1-s intervals. The failure modes of the columns involved overall flexural buckling and combined local and overall buckling. The full load-lateral displacement curves were recorded and are shown in Figs. 13 and 14 for the SHS and RHS specimens, respectively. Key results from the tests, including the static ultimate load N_u and the lateral displacement at ultimate load ω_u, are reported in Table 11.

Analysis of Results and Design Recommendations

Cross Section Classification

In the European structural stainless steel design standard Eurocode 3: Part 1-4 (CEN 2006a), the concept of cross section classification is

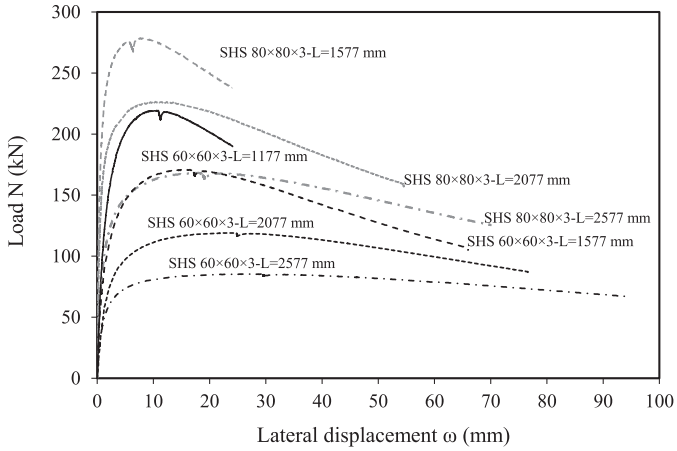

Fig. 13. SHS $80 \times 80 \times 3$ and SHS $60 \times 60 \times 3$ load-lateral displacement curves

J. Struct. Eng. 2013.139:717-728.

used for the treatment of local buckling. The method assumes elastic-perfectly plastic material behavior for stainless steel as for carbon steel in Eurocode 3: Part 1-1 (CEN 2005), with the yield stress taken as the 0.2% proof stress. The classification of plate elements in cross sections is based on the width-to-thickness ratio (b/t), the material properties $[(235/f_y)(E/210{,}000)]^{0.5}$, the edge support conditions (i.e., internal or outstand referred to as stiffened and unstiffened, respectively, in the North American specification), and the form of the applied stress field. The overall cross section classification is assumed to relate to its most slender constituent element. The definition of the four classes used in Eurocode 3: Part 1-4 is as follows: Class 1 cross sections are fully effective under pure compression and capable of reaching and maintaining their full plastic moment M_{pl} in bending; Class 2 cross sections have a somewhat lower deformation capacity but are also fully effective in pure compression and capable of reaching their full plastic moment in bending; Class 3 cross sections are fully effective in pure compression but local buckling prevents attainment of the full plastic moment in bending, limiting its bending resistance to the elastic moment M_{el}; and Class 4 cross sections are characterized as slender and cannot reach their nominal yield strength in compression or their elastic moment capacity in bending; to reflect this, regions of the sections rendered ineffective by local buckling are removed, and section properties are calculated on the basis of the remaining cross section.

The North American SEI/ASCE-8 (ASCE 2002) specification for the design of cold-formed stainless steel structures uses a similar approach for cross sections in compression and calculates the moment capacity either on the basis of initiation of yielding (Procedure I) or on the basis of the inelastic reserve capacity (Procedure II). Procedure I assumes a linear stress distribution throughout the cross section with the yield stress being the maximum allowable stress. A maximum slenderness limit, equivalent to the Eurocode 3: Part 1-4 Class 3 limit, is provided, beyond which loss of effectiveness caused by local buckling needs to be accounted for through the use of effective section properties. The additional inelastic reserve capacity associated with stockier cross sections, up to a maximum slenderness limit equivalent to the Eurocode 3: Part 1-4 Class 1 limit, may be used through the application of the Procedure II design method, provided certain criteria regarding web slenderness, cross section geometry, shear stresses, and the elimination of other possible failure modes are satisfied.

In this section, the experimental results are used to assess the applicability of the cross section classification limits provided in the current European (EN 1993-1-4; CEN 2006a) and North American (SEI/ASCE-8; ASCE 2002) standards to ferritic stainless steel internal elements. In addition, the proposed limits of Gardner and Theofanous (2008), which are derived and statistically validated based on all relevant published test data on stainless steel, are also considered. The measured weighted average material properties from the flat tensile coupon tests for each cross section were used throughout the analyses.

Both the stub column tests results and the bending tests results have been used to assess the suitability of the Class 3 slenderness limit for internal elements in compression. Figs. 15 and 16 show the relevant response characteristics ($N_u/A\sigma_{0.2}$ and M_u/M_{el}), where N_u and M_u are the ultimate test load and moment, respectively, and M_{el} is the conventional elastic moment capacity, given as the product of the elastic section modulus and the yield strength, plotted against the slenderness parameter $c/t\varepsilon$ of the most slender constituent element in the cross section, where c is the compressed flat width, t is the element thickness, and $\varepsilon = [(235/f_y)(E/210{,}000)]^{0.5}$, as defined in EN 1993-1-4 (CEN 2006a). In determining the most slender element, an account of the stress distribution and element support conditions has been made through the buckling factor k_σ, as defined in EN 1993-1-5 (CEN 2006b). The Class 3 limit specified in

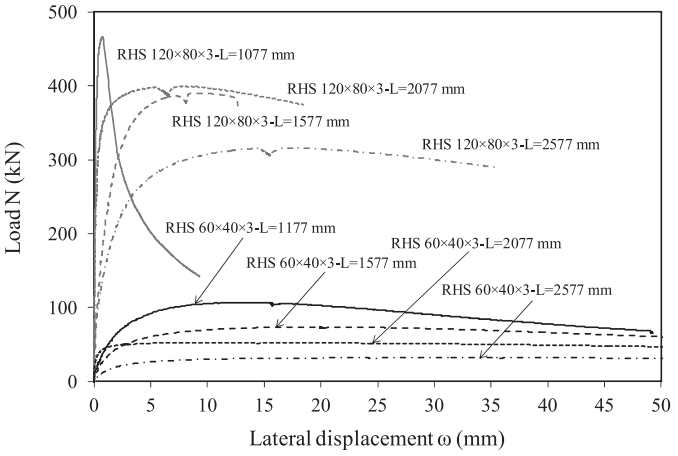

Fig. 14. RHS $120 \times 80 \times 3$ and RHS $60 \times 40 \times 3$ load-lateral displacement curves

Table 11. Summary of Results from Column Flexural Buckling Tests

Specimen	Axis of buckling	N_u (kN)	ω_u (mm)
RHS $120 \times 80 \times 3$-1077	Major	463	0.77
RHS $120 \times 80 \times 3$-1577	Major	382	9.36
RHS $120 \times 80 \times 3$-2077	Major	391	7.87
RHS $120 \times 80 \times 3$-2577	Major	308	18.27
RHS $60 \times 40 \times 3$-1177	Minor	103	12.72
RHS $60 \times 40 \times 3$-1577	Minor	72	19.62
RHS $60 \times 40 \times 3$-2077	Minor	51	8.78
RHS $60 \times 40 \times 3$-2577	Minor	30	30.50
SHS $80 \times 80 \times 3$-1577	—	273	7.75
SHS $80 \times 80 \times 3$-2077	—	222	10.39
SHS $80 \times 80 \times 3$-2577	—	164	18.03
SHS $60 \times 60 \times 3$-1177	—	214	10.82
SHS $60 \times 60 \times 3$-1577	—	166	15.64
SHS $60 \times 60 \times 3$-2077	—	116	23.95
SHS $60 \times 60 \times 3$-2577	—	82	24.82

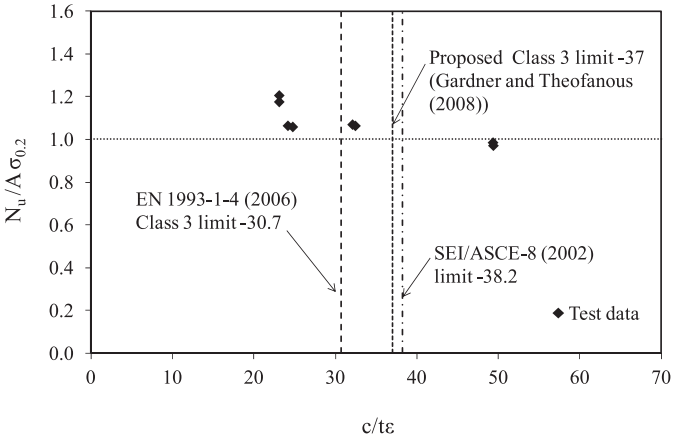

Fig. 15. Assessment of Class 3 slenderness limits for internal elements in compression (stub column tests)

J. Struct. Eng. 2013.139:717-728.

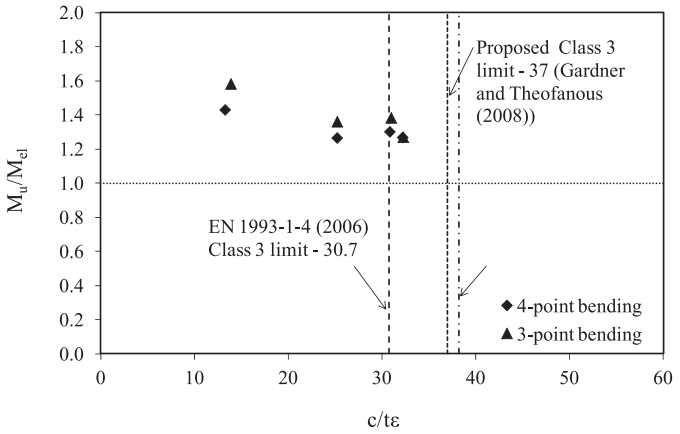

Fig. 16. Assessment of Class 3 slenderness limits for internal elements in compression (bending tests)

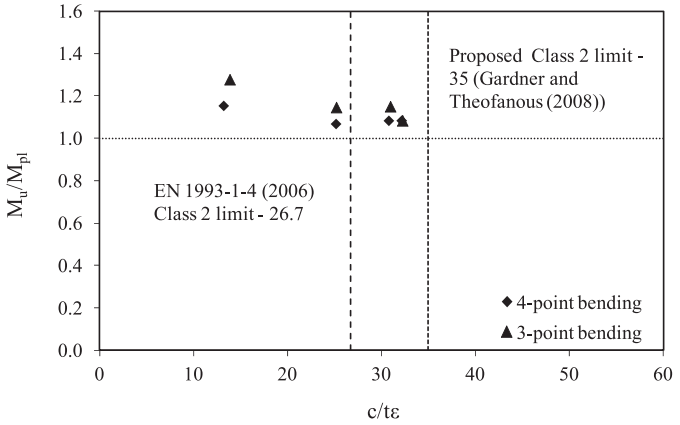

Fig. 17. Assessment of Class 2 slenderness limits for internal compression elements

Eurocode 3: Part 1-4 is 30.7, whereas the equivalent Class 3 limit of the SEI/ASCE-8 is 38.2. The Class 3 slenderness limit proposed by Gardner and Theofanous (2008) is 37, which is very close to the slenderness limit of 38.3 from SEI/ASCE-8 (ASCE 2002). From Figs. 15 and 16, it may be concluded that the current Class 3 limit given in EN 1993-1-4 (CEN 2006a) is applicable to ferritic stainless steel internal elements under compression but is rather conservative, whereas the SEI/ASCE-8 (ASCE 2002) limit and the proposed limit of Gardner and Theofanous (2008) allow more efficient exploitation of the material.

The Class 2 slenderness limits specified in EN 1993-1-4 (CEN 2006a) and proposed by Gardner and Theofanous (2008), together with the bending test results, are shown in Fig. 17, where the test ultimate moment capacity M_u has been normalized by the plastic moment capacity M_{pl}, given as the product of the plastic section modulus and the yield strength and plotted against the slenderness parameter $c/t\varepsilon$ of the most slender constituent element in the cross section. In Fig. 18, the rotation capacity R is plotted against the slenderness parameter $c/t\varepsilon$ of the most slender constituent element in the cross section. In the absence of a codified deformation capacity requirement for Class 1 stainless steel cross sections, the equivalent carbon steel rotation capacity requirement of $R = 3$ (Sedlacek and Feldmann 1995) has been used herein. From Fig. 17, the EN 1993-1-4 (CEN 2006a) Class 2 limit of 26.7 may be seen to be safe, whereas the

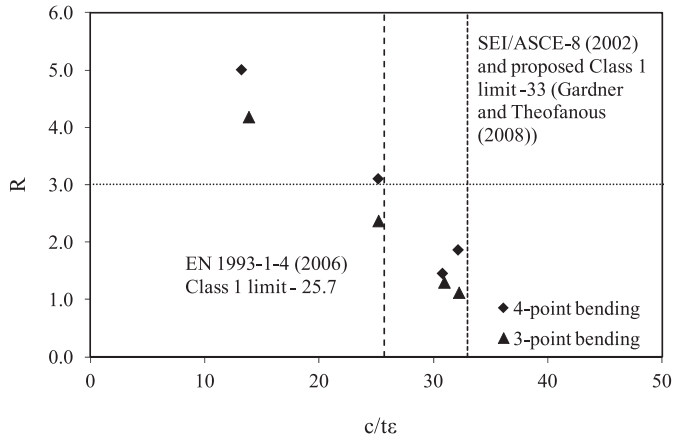

Fig. 18. Assessment of Class 1 slenderness limits for internal compression elements

proposed limit of 35 (Gardner and Theofanous 2008) provides more economical structural design. The SEI/ASCE-8 (ASCE 2002) equivalent Class 1 limit, which is the same as the corresponding limit proposed by Gardner and Theofanous (2008), appears optimistic for ferritic stainless steel, and the EN 1993-1-4 (CEN 2006a) provisions may be adopted.

Flexural Buckling

The Eurocode 3: Part 1-4 (CEN 2006a) design approach for flexural buckling of compression members is based on the Perry-Robertson buckling formulation with a linear imperfection parameter $\eta = \alpha(\overline{\lambda} - \overline{\lambda}_0)$, where α and $\overline{\lambda}_0$ are constants accounting for the geometric imperfections and residual stresses effects on the column strength. The design buckling curves were derived by calibration against the then available stainless steel test data to provide a suitably conservative fit for design purposes. A single buckling curve is provided for cold-formed open and rolled tubular sections of austenitic, duplex, and ferritic stainless steel grades. For simplicity, to avoid the need for iteration and for consistency with the carbon steel approach, no explicit allowance is made for the effect of gradual material yielding in the member buckling formulations. In contrast, the SEI/ASCE-8 (ASCE 2002) provisions for stainless steel column design allow for the nonlinear stress-strain response through the use of the tangent modulus E_t, corresponding to the buckling stress, in place of the initial modulus E in the buckling formulations, which involves an iterative design approach.

In addition to the iterative method from the SEI/ASCE-8 (ASCE 2002) specification, an alternative explicit design procedure is also provided in the AS/NZS 4673 [Australian/New Zealand Standard (AS/NZS) 2001] standard for cold-formed stainless steel structures. The method is essentially the same as the Eurocode 3: Part 1-4 (CEN 2006a) formulation for flexural buckling of compression members, except that a nonlinear expression is used for the imperfection parameter instead of the linear expression adopted in Eurocode 3: Part 1-4 (CEN 2006a). In addition, a total of six buckling curves are provided for different stainless steel grades: austenitic (EN 1.4301, 1.4401, 1.4306, and 1.4404), ferritic (EN 1.4512, 1.4003, and 1.4016), and duplex (EN 1.4462). In this section, the results of the ferritic stainless steel column flexural buckling tests performed herein are examined and compared with the current column design provisions adopted in the European, North American, and Australian/New Zealand standards.

J. Struct. Eng. 2013.139:717-728.

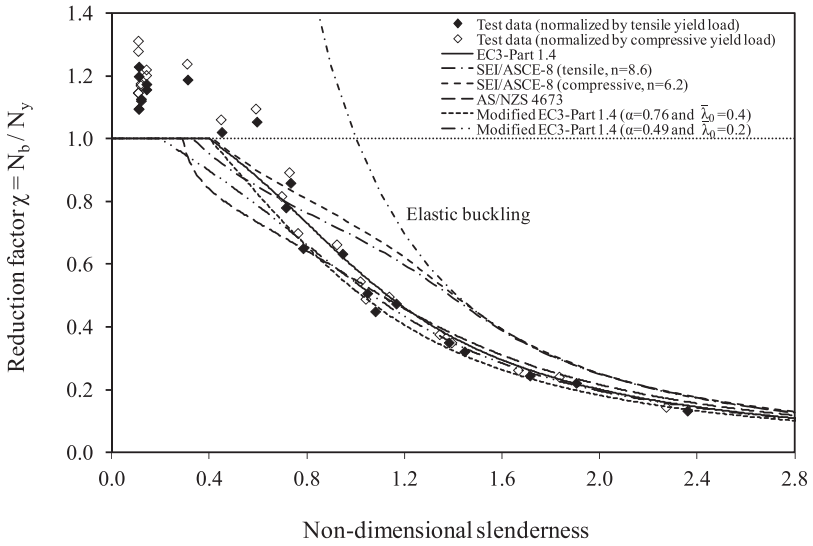

Fig. 19. Flexural buckling test results and code comparisons

In Fig. 19, the test ultimate loads normalized by the corresponding tensile and compressive squash loads, based on the gross cross-sectional area for fully effective sections and the effective cross-sectional area A_{eff} for slender sections, have been plotted against the nondimensional slenderness $\bar{\lambda}$ as defined in Eq. (2). Stub column test data are also included. The SEI/ASCE-8 buckling curves, based on the mean measured tensile and compressive flat weighted average material properties of the tested sections, together with the EC3: Part 1-4 buckling curve for cold-formed hollow sections, with the imperfection factor $\alpha = 0.49$ and $\bar{\lambda}_0 = 0.4$ as specified in Eurocode 3: Part 1-4 (CEN 2006a), are also depicted. The AS/NZS buckling curve for grade EN 1.4003 is also included. To allow suitable comparison with the test data, measured geometry and material properties are adopted, and all codified factors of safety are set to unity.

As shown in Fig. 19, the SEI/ASCE-8 curves are the highest over most of the slenderness range and generally overpredict the test results. The AS/NZS curve is below the EC4: Part 1-4 buckling curve in the low and intermediate slenderness ranges, with both curves meeting at a slenderness value of approximately 1.2 and converging toward the elastic buckling curve at higher slenderness. Overall, the EC3: Part 1-4 buckling curve provides a better representation of the member buckling resistance over the full slenderness range, though a number of data points fall below the curve. Alternative buckling curves, with either a higher imperfection factor and the current plateau length ($\alpha = 0.76$ and $\bar{\lambda} = 0.4$) or a shorter plateau and the current imperfection factor ($\alpha = 0.49$ and $\bar{\lambda} = 0.2$) provide a better approximation to the test results.

Comparison with Other Stainless Steel Grades

Test data collected from the literature (Rasmussen and Hancock 1993a, b; Talja and Salmi 1995; Ala-Outinen and Oksanen 1997; Kuwamura 2003; Liu and Young 2003; Young and Liu 2003; Gardner and Nethercot 2004a, b; Real and Mirambell 2005; Young and Lui 2005; Zhou and Young 2005; Gardner et al. 2006; Young and Lui 2006; Theofanous and Gardner 2009; Gardner and Theofanous 2010; Theofanous and Gardner 2010) on austenitic, duplex, and lean duplex stainless steel SHS and RHS specimens have been used to compare with the test results generated herein and to assess the relative performance of various stainless steel grades. In Fig. 20, the reported ultimate load capacity from stub column tests have been

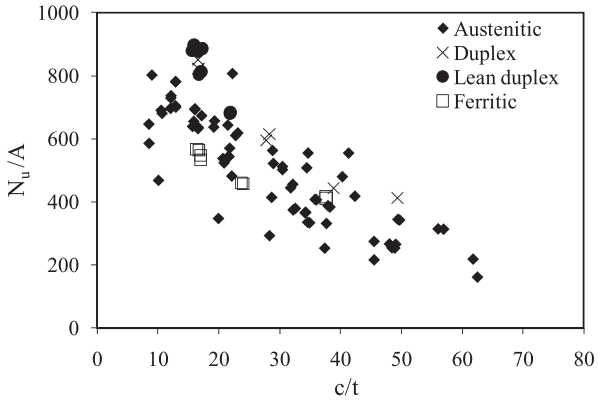

Fig. 20. Performance of stub columns of various stainless steel grades

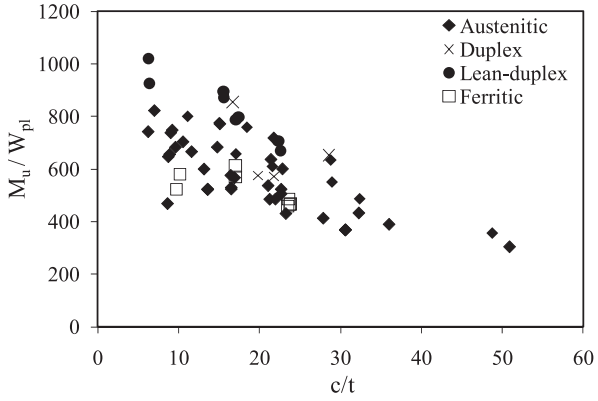

Fig. 21. Performance of beams of various stainless steel grades

normalized by the respective cross-sectional area and plotted against the *c*/*t* ratio of the most slender element in the section. The bending tests results reported herein were also compared with tests on other stainless steel grades as shown in Fig. 21, where the ultimate moment capacity normalized by the respective plastic section modulus is plotted against the *c*/*t* ratio of the compression flange of the cross

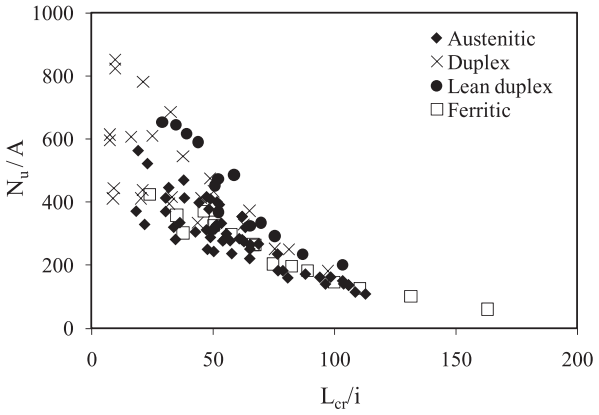

Fig. 22. Performance of columns of various stainless steel grades

section. The collected column flexural buckling data are presented in Fig. 22, where the member slenderness is calculated based on the geometric properties of the gross cross sections. The experimental data presented in Figs. 20–22 exhibit the general anticipated trend of reducing failure stress with increasing slenderness. The vertical scatter for a given slenderness reflects the variation in material strength between the tested specimens. Overall, of the grades considered, lean duplex specimens generally show the highest failure stress, which is in line with the high yield strength associated with this material, whereas the results of the other grades overlap.

Conclusions

A laboratory testing program has been conducted at Imperial College London to investigate the structural performance of cold-formed ferritic stainless steel tubular structural elements. Eight stub column tests, 15 flexural buckling tests, eight beam tests and a total of 36 material tests have been reported herein. The experimental results were used to assess the applicability of the European (EN 1993-1-4; CEN 2006a) and North American (SEI/ASCE-8; ASCE 2002) provisions to ferritic stainless steel structural components. It was concluded that the current Class 3 slenderness limits provided in EN 1993-1-4 (CEN 2006a) is applicable to ferritic stainless steel internal elements under compression, while the SEI/ASCE-8 (ASCE 2002) equivalent limit and the proposed limit of Gardner and Theofanous (2008) allow greater design efficiency. Similarly, the EN 1993-1-4 (CEN 2006a) Class 2 limit was considered to be safe whereas the more relaxed limit of Gardner and Theofanous (2008) provides more economical structural design. The SEI/ASCE-8 (ASCE 2002) equivalent Class 1 limit and that proposed by Gardner and Theofanous (2008) appeared to be optimistic for ferritic stainless steel; hence, the EN 1993-1-4 (CEN 2006a) limit was recommended in this paper. It was concluded that although the EC3: Part 1-4 column buckling curve provides a better representation of the member buckling resistance over the full slenderness range, its proposed modified versions provide a better approximation to the buckling resistance exhibited by the test specimens. The laboratory test results on ferritic stainless steel were also compared with test results on austenitic, duplex and lean duplex stainless steel SHS and RHS specimens collected from the literature. Overall, ferritic stainless steel shows similar structural performance to other commonly used stainless steel grades and at a lower material cost, making it an attractive choice for structural applications.

Notation

The following symbols are used in this paper:

A = cross-sectional area;
A_c = coupon cross-sectional area;
A_{eff} = effective cross-sectional area;
b = width;
E = Young's modulus;
h = depth;
i = radius of gyration;
k_σ = buckling coefficient;
L = member length;
L_{cr} = column buckling length;
M_{el} = elastic moment capacity;
M_{pl} = plastic moment capacity;
M_u = test ultimate moment;
N = load;
N_b = column buckling load;
N_{cr} = elastic buckling load;
N_u = test ultimate load;
N_y = yield load;
n = strain hardening component used in Ramberg-Osgood model;
$n'_{0.2,1.0}$ = strain hardening component used in compound Ramberg-Osgood model;
R = rotation capacity;
r_i = internal corner radius;
t = thickness;
w_0 = maximum measured local imperfection;
δ_u = stub column end shortening at ultimate load;
ε = material factor defined in EN 1993-1-4 (CEN 2006b);
ε_f = strain at fracture;
θ = rotation;
θ_{pl} = elastic part of the total rotation at midspan when M_{pl} is reached on the ascending branch;
θ_u = total rotation at midspan when the moment-rotation curve falls below M_{pl} on the descending branch;
κ = curvature;
κ_{pl} = elastic part of the total curvature at midspan when M_{pl} is reached on the ascending branch;
κ_u = total curvature at midspan when the moment-curvature curve falls below M_{pl} on the descending branch;
$\overline{\lambda}$ = member slenderness;
σ = stress;
$\sigma_{0.2}$ = 0.2% proof stress;
$\sigma_{1.0}$ = 1.0% proof stress;
σ_u = ultimate tensile stress;
ω = lateral deflection;
ω_u = lateral deflection at ultimate load; and
ω_0 = initial global imperfection amplitude.

Acknowledgments

The authors are grateful to the Outokumpu Research Foundation and the Steel Construction Institute for their financial contributions to the project and Stalatube Finland for providing the test specimens and thank Gordon Herbert and Angeliki Ntikmpasani for assistance during the experimental investigations.

J. Struct. Eng. 2013.139:717-728.

References

Ala-Outinen, T., and Oksanen, T. (1997). "Stainless steel compression members exposed to fire." *Research note 1864*, Valtion Teknillisestä Tutkimuslaitoksesta (VTT) Building Technology, Helsinki, Finland.

ASCE. (2002). "Specification for the design of cold-formed stainless steel structural members." *SEI/ASCE 8-02,* Reston, VA.

Ashraf, M., Gardner, L., and Nethercot, D. A. (2005). "Strength enhancement of the corner regions of stainless steel cross-sections." *J. Constr. Steel Res.*, 61(1), 37–52.

Ashraf, M., Gardner, L., and Nethercot, D. A. (2006). "Finite element modelling of structural stainless steel cross-sections." *Thin-Walled Struct.*, 44(10), 1048–1062.

Australian/New Zealand Standard. (2001). "Cold-formed stainless steel structures." *AS/NZS 4673:2001*, Sydney, Australia.

Blue-hill 2 [Computer software]. High Wycombe, U.K, Instron.

Centre for Advanced Structural Engineering. (1990). "Compression tests of stainless steel tubular columns." *Investigation Rep. S770,* Univ. of Sydney, Sydney, Australia.

European Committee for Standardization (CEN). (2005). "Design of steel structures: Part 1-1: General rules and rules for buildings." *Eurocode 3, EN 1993-1-1*, Brussels, Belgium.

European Committee for Standardization (CEN). (2006a). "Design of steel structures: Part 1-4: General rules: Supplementary rules for stainless steel." *Eurocode 3, EN 1993-1-4*, Brussels, Belgium.

European Committee for Standardization (CEN). (2006b). "Design of steel structures: Part 1-5: Plated structural elements." *Eurocode 3, EN 1993-1-5*, Brussels, Belgium.

European Committee for Standardization (CEN). (2009a). "Metallic materials —tensile testing—Part 1: Method of test at room temperature." *EN ISO 6892-1*, Brussels, Belgium.

European Committee for Standardization (CEN). (2009b). "Stainless steels: Part 4: Technical delivery conditions for sheet/plate and strip of corrosion resisting steels for general purposes." *EN 10088-4*, Brussels, Belgium.

Galambos, T. V. (1998). *Guide to stability design criteria for metal structures*, 5th Ed., Wiley, New York.

Gardner, L., and Nethercot, D. A. (2004a). "Experiments on stainless steel hollow sections—Part 1: Material and cross-sectional behaviour." *J. Constr. Steel Res.*, 60(9), 1291–1318.

Gardner, L., and Nethercot, D. A. (2004b). "Experiments on stainless steel hollow sections—Part 2: Member behaviour of columns and beams." *J. Constr. Steel Res.*, 60(9), 1319–1332.

Gardner, L., Talja, A., and Baddoo, N. R. (2006). "Structural design of high-strength austenitic stainless steel." *Thin-Walled Struct.*, 44(5), 517–528.

Gardner, L., and Theofanous, M. (2008). "Discrete and continuous treatment of local buckling in stainless steel elements." *J. Constr. Steel Res.*, 64(11), 1207–1216.

Gardner, L., and Theofanous, M. (2010). *Plastic design of stainless steel structures*, *Proc. of Int. Colloquium on Stability and Design of Steel Structures*, SDSS Rio 2010, Federal Univ. of Rio de Janiero and the State Univ. of Rio de Janiero, Brazil, 665–672.

Kuwamura, H. (2003). "Local buckling of thin-walled stainless steel members." *Steel Struct.*, 3(3), 191–201.

Liu, Y., and Young, B. (2003). "Buckling of stainless steel square hollow section compression members." *J. Constr. Steel Res.*, 59(2), 165–177.

Mirambell, E., and Real, E. (2000). "On the calculation of deflections in structural stainless steel beams: An experimental and numerical investigation." *J. Constr. Steel Res.*, 54(1), 109–133.

Rasmussen, K. J. R., and Hancock, G. J. (1993a). "Design of cold-formed stainless steel tubular members. I: Columns." *J. Struct. Eng.*, 119(8), 2349–2367.

Rasmussen, K. J. R., and Hancock, G. J. (1993b). "Design of cold-formed stainless steel tubular members. II: Beams." *J. Struct. Eng.*, 119(8), 2368–2386.

Rasmussen, K. J. R. (2003). "Full-range stress–strain curves for stainless steel alloys." *J. Constr. Steel Res.*, 59(1), 47–61.

Real, E., and Mirambell, E. (2005). "Flexural behavior of stainless steel beams." *Eng. Structures*, 27(10), 1465–1475.

Schafer, B. W., and Peköz, T. (1998). "Computational modeling of cold-formed steel: characterizing geometric imperfections and residual stresses." *J. Constr. Steel Res.*, 47(3), 193–210.

Sedlacek, G., and Feldmann, M. (1995). "The b/t-ratios controlling the applicability of analysis models in Eurocode 3, Part 1.1. Background Document 5.09 for chapter 5 of Eurocode 3, Part 1.1." Aachen, Germany.

Talja, A., and Salmi, P. (1995). "Design of stainless steel RHS beams, columns and beam-columns." *Research note 1619*, Valtion Teknillisestä Tutkimuslaitoksesta (VTT) Building Technology, Helsinki, Finland.

Theofanous, M., and Gardner, L. (2009). "Testing and numerical modeling of lean duplex stainless steel hollow section columns." *Eng. Structures*, 31(12), 3047–3058.

Theofanous, M., and Gardner, L. (2010). "Experimental and numerical studies of lean duplex stainless steel beams." *J. Constr. Steel Res.*, 66(6), 816–825.

van den Berg, G. J. (2000). "The effect of non-linear stress-strain behavior of stainless steels on member capacity." *J. Struct. Eng.*, 135(1), 135–160.

Young, B., and Liu, Y. (2003). "Experimental investigation of cold-formed stainless steel columns." *J. Struct. Eng.*, 129(2), 169–176.

Young, B., and Lui, W. M. (2005). "Behavior of cold-formed high strength stainless steel sections." *J. Struct. Eng.*, 131(11), 1738–1745.

Young, B., and Lui, W. M. (2006). "Tests on cold formed high strength stainless steel compression members." *Thin-Walled Struct.*, 44(2), 224–234.

Zhou, F., and Young, B. (2005). "Tests of cold-formed stainless steel tubular flexural members." *Thin-Walled Struct.*, 43(9), 1325–1337.

J. Struct. Eng. 2013.139:717-728.